The Visual Computer

The synthesis of rust in seawater

Yao-Xun Chang,
Zen-Chung Shih

Department of Computer and Information Science, National Chiao Tung University, Hsinchu, 30050, Taiwan, R.O.C.
E-mail: gis82548@cis.nctu.edu.tw, zcshih@cc.nctu.edu.tw

Published online: 28 January 2003

Computer graphics researchers have recently revealed that the presence of imperfections is an essential part of the illusion of photorealism. An improved model to simulate the rust development of ferrous metals in seawater is proposed. The tide and the current, under the gravity of the sun and the moon, affect the stability of the environment at the bottom of the ocean. A simple current model is employed to elucidate the periodic transition of currents in the ocean. L-systems, coupled with the current model, modulate the diffusion of rust according to tendencies based on the object geometry and environmental factors. Changing the underlying distributions of tendency allows images of a variety of metallic rusts to be generated.

Key words: Texture synthesis – Metallic corrosion – L-systems

1 Introduction

Although rendering techniques such as ray tracing and radiosity algorithms – which simulate light and its interaction with the environment – can enhance a virtual scene using effects such as soft shadows and reflections, the illusion of photorealism also depends crucially on the quality of the underlying material models. Over the past decade, researchers have attempted to model the changes in the appearance of a surface due to aging phenomena, such as dirt accumulation, rain washing, sedimentation of deposits, and metal corrosion (Becket and Badler 1990; Blinn 1982; Chang and Shih 2000; Dorsey el al. 1999; Dorsey and Hanrahan 1996; Dorsey et al. 1996; Gobron and Chiba 1999; Hsu and Wong 1995; Merillou et al. 2001; Miller 1994; Wong et al. 1997). Such investigations have sought to enhance the authenticity of computer-generated images, because digitally created objects in early computer images looked too clean to be realistic. Accordingly, methods for generating various imperfections on a surface have been elucidated, showing that the presence of imperfections is critical in causing a viewer to accept willingly the rendered images as real. The appearance of a real surface can change over time when exposed to the surrounding environment. Real-world objects are normally covered with a variety of imperfections that underlie a person perceiving the object as real. Therefore, this study concentrates on elucidating the basic physical models of aging phenomena and modeling the corresponding evolution of a surface.

Imperfections may occur for a number of reasons that range from chemical reactions, such as metallic rusting, to biological growth, such as the covering of a stone with moss. Many pieces of research have proposed to the simulation of related aging and weathering effects. Becket and Badler (1990) generated a broad class of surface blemishes, such as scratches and splotches. Miller (1994) related surface accessibility to the distribution of patinas on tarnished surfaces. Hsu and Wong (1995) simulated the amount of dust accumulation. Furthermore, Wong et al. (1997) proposed a geometry-dependent method to represent blemishes according to modeled tendency distribution. Dorsey and Hanrahan (1996) examined a metallic surface as a series of layers and then simulated the patina with a collection of procedural operators. Dorsey et al. (1999) also modeled the patterns of washes and weathered stone. Gobron and Chiba (1999) described a 3D-surface cellular au-

Digital Object Identifier (DOI) 10.1007/s00371-002-0172-0

tomata method, simulating the propagation of patinas over surfaces. More recently, Merillou et al. (2001) provided an approach based on experimental data to simulate and render the corrosion (rusting) of metals.

In light of the above developments, our previous work presented a physically based model to simulate the appearance of patinas on antique objects that have for a long time been underground, including ancient Chinese bronzes (Chang and Shih 2000). The framework presented simulates the development of layered patinas guided by environmental tendencies. The distributions of tendency (Wong et al. 1997) representing the potential occurrence of patinas were defined to model the influence of environmental factors on patination. The structure of patinas was represented as a set of layers. This approach, as well as using a simple rule-based algorithm to simulate the complicated diffusion of different patinas, has the advantage of incorporating the influence of the environment on patinas. The primary concern in simulating patinas on ancient Chinese bronzes is the bronzes' burial environment. The underground environment is well known to be almost static. Any changes to the antiques are small. Accordingly, invariable distributions are assumed throughout the simulation in our model. The model used these distributions to determine the propagation of various patinas without updating any tendency values. However, not all real environments remain static; for instance, the atmosphere and the ocean provide dynamic environments. The formation of corrosion products influences subsequent corrosion processes, meaning that the formation changes the corrosive potential of the immediate environment of the products. Thus, this paper develops an enhanced environment module to describe dynamic environments such as seawater. Feedback to the environment of newly formed corrosion products is also included in the new model presented here, to imitate precisely the interaction between the material and the surrounding environment.

This study extends the authors' previous patination model to generate the rusty appearance of ferrous metals in seawater, as shown in Fig. 1. The proposed model consists of two modules – a *seawater module* and a *rusting module*. The seawater module adopts tendency distributions to reflect the potential of rusting in seawater. The rusting module simulates the development of the diffusion of the rust. A simple current model is employed to illustrate the periodic transition of currents in the ocean. Coupling the current model with the order of iteration, the rusting module models the diffusion of rust on surfaces according to the change of a dynamic environment. Following each iteration of the L-system, the environment module updates tendency values of vertices at which rusting occurs. Dormancy is accounted for in the rusting module. Rust development may be held in abeyance, or remain torpid under ill-suited conditions, and begin propagating again as circumstances become favorable owing to the dynamic nature of tendency distributions. Finally, the symbol string generated by L-systems is graphically interpreted by a ray tracer.

Fig. 1. Samples of real metallic rust in seawater

The rest of this paper is organized as follows. Section 2 briefly describes the underlying characteristics of seawater during rusting and the formation of rust in such an environment. Section 3 specifies the overall descriptive framework for interactions between rust and environment. Section 4 presents the distribution of tendencies that maps the influence of various factors on the development of rust. Section 5 depicts the L-system, simulating the effect of the environment on the growth of rust. Section 6 discusses a visualization method that renders the blemished model. Section 7 gives experimental results that demonstrate the proposed framework, while conclusions and areas for further research are finally provided in Sect. 8.

2 The rusting in seawater

Research in the field of corrosion (Craig 1989; Fontana 1986; Jones 1992; Newman and Sieradzki 1994; Ross 1977; Shreir 1976) has revealed that the chemical properties of a given metal depend on the precise prevailing environmental conditions. Corrosion can be basically considered to be a heterogeneous chemical reaction that occurs at a metal–environment interface. The rusting of ferrous metals – one kind of corrosion – is an electrochemical process that can be broken down into anodic and cathodic reactions (Chandler 1985; Fontana 1986; Jones 1992; Rogers 1968; Ross 1977; Shreir 1976). The products of anodic and cathodic reactions, Fe^{2+} and OH^- respectively, migrate in the electrolyte and react to form ferrous hydroxide that is eventually oxidized to ferric salt: $Fe^{2+} + 2OH^- \rightarrow Fe(OH)_2 \rightarrow Fe_2O_3 \cdot H_2O$. Where the supply of oxygen is restricted, black Fe_3O_4 is formed. This description is simplified but serves to illustrate the electrochemical process of rusting and the essential role of moisture and oxygen supplied by the environment. Exactly how seawater influences rusting must be investigated to support a lifelike simulation of rusting in the sea.

2.1 Seawater

Seawater is a common environment in which metallic products are exposed. The chloride content of seawater supports an electric conductivity much higher than that of air, possibly leading to higher corrosivity. In fact, the corrosive nature of seawater is also affected by the concentration and availability of dissolved oxygen, the salinity, the concentration of minor ions, and the concentration and nature of pollutants. Other factors, including temperature, depth and ocean currents, are often equally or more important. However, not all factors that govern corrosion can be easily isolated and measured.

- *Dissolved gases*. Oxygen and carbon dioxide are the most important gases dissolved in seawater. At ordinary temperatures, dissolved oxygen is a prerequisite for any appreciable corrosion of iron or steel. Moreover, differences in dissolved oxygen transport readily generate differential aeration cells, resulting in localized corrosion on the iron surface. Carbon dioxide significantly affects the pH of seawater and influences the formation of protective carbonate scales. In seawater, the bicarbonate ions form insoluble calcareous scales, resulting from cathodic protection. These coherent and adherent scales limit access by dissolved oxygen, markedly reducing the rate of corrosion.
- *pH*. In the intermediate pH4 through pH10 range, a loose, porous ferrous-oxide deposit shields the metal surface. The rate of corrosion is nearly constant. In solutions more acidic than pH4, oxide is soluble and corrosion increases owing to the availability of H^+ ions. At pH values exceeding 10, corrosion is slow due to the formation of a passive ferric oxide film in dissolved oxygen.
- *Temperature*. Changes in temperature alter the rate at which chemical and electrochemical reactions proceed. For example, a rise in temperature would be expected to lead to an increase in corrosion. However, such a rise also decreases the solubility of the dissolved oxygen, thereby promoting the formation of a protective magnetite film on surfaces. The temperature of seawater is subject to seasonal variations depending on the prevailing winds, ocean currents, tidal streams and elevation of the sun.
- *Depth*. Oxygen varies with an increasing depth, tending to drop from 1000 m to 2000 m and then increase again. The temperature declines with depth. The rate of corrosion generally decreases with depth. Apart from the general corrosion rate, factors such as pressure and mechanical effects varying with the depth may be important in determining the types of corrosion that occur.
- *Velocity*. The velocity of seawater can markedly influence corrosion by controlling the supply of oxygen to the rusting surface and removing products that would otherwise stifle further rusting. The motion of water may cause the formation of differentially aerated cells. Several specific forms of corrosion, such as cavitation, can manifest at high seawater velocities. Corrosion in seawater increases with velocity, because of the high concentration of chloride ions.

2.2 Forms of corrosion

Corrosion can affect metals in a variety of ways, depending on its type and the precise prevailing environmental conditions. Corrosion can range from fairly uniform wastage, resulting in general thinning, to highly localized attack, resulting in pitting

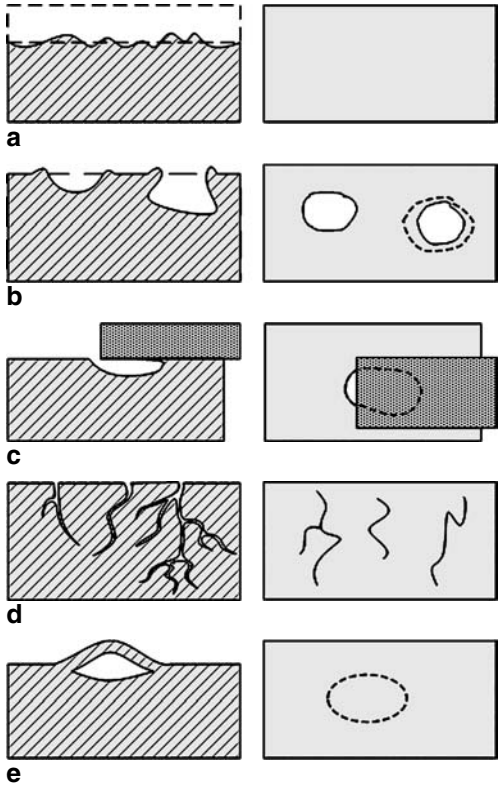

Fig. 2a–e. Different types of corrosion: **a** uniform corrosion; **b** pitting; **c** crevice corrosion; **d** stress corrosion crack; **e** hydrogen blister (*left column* is the cross-section, *right column* is exposed surfaces)

and cracking. As such, various forms of corrosion have been categorised according to the appearance of the corroded metal (Chandler 1985; Fontana 1986; Jones 1992; Rogers 1971; Trethewey and Chamberlain 1988). Figure 2 schematically depicts several typical forms of corrosion.

- *Uniform corrosion*. A uniform, regular removal of metal from a surface is the most common form of corrosion and is typified by steel rusting. "Uniform" implies that a chemical or electrochemical reaction proceeds over the entire exposed surface at approximately the same rate, but the loss of metal is rarely completely uniform.
- *Pitting corrosion*. Pitting is a form of extremely localized attack that penetrates small, discrete areas. Commonly, the penetration through the surface is deeper than that caused by uniform corrosion. All aqueous environments can support this kind of attack and no metal is immune from it. Although the likelihood and course of pitting is always unpredictable, some conditions encourage pitting, such as (1) the presence of chlorides, (2) stagnant conditions, and (3) discontinuities in protective coatings.
- *Crevice corrosion*. This type of corrosion usually occurs where a crevice is formed between two surfaces, such as in lapped joints, under washers and in loose bolts. Crevice corrosion results simply from differences between the metal ion or oxygen concentration in the crevice and that in its surroundings. A large cathodic current acting on the small anodic area in the crevice facilitates an intense local attack.
- *Stress corrosion crack*. Stress corrosion cracking occurs under a static tensile stress within specific corrosive environmental conditions. For example, stainless steel is susceptible in hot chlorides and carbon steel in nitrates. Such corrosion can lead to rapid failure of an alloy. The major factors that influence such corrosion include the environmental conditions, the stress conditions and the alloy under consideration. However, the mechanisms involved are not well understood.
- *Hydrogen blister*. A hydrogen blister is formed when atomic hydrogen migrates from the surface to internal defects and voids, in which molecular hydrogen can nucleate, generating sufficient internal pressure locally to deform and rupture the metal. This process normally occurs in storage tanks and in refining processes.

This work represents metallic rust as patinas – that is, as a series of layers (Dorsey and Hanrahan 1996) with zero thickness and with each layer containing at least one corrosion form, as illustrated in Fig. 3. The lowest layer on the base metal is the oxide layer, and is composed of two chemical constituents – reddish hematite and black magnetite. The next layer is the hydrogen blister that simulates the bubbles formed between the oxide layer and the base metal. This layer deforms surface geometry, but does not change the constituents of the rust. A deposition layer immediately next to the blister layer is formed when dissociated ferrous ions in seawater react with salts such as carbonates and sulfates. Pitting and cracking are feathering in the top layer. The upper three layers need not coexist; for example, pits or cracks may be observed directly on the oxide layer. However, the sequence of these layers cannot change.

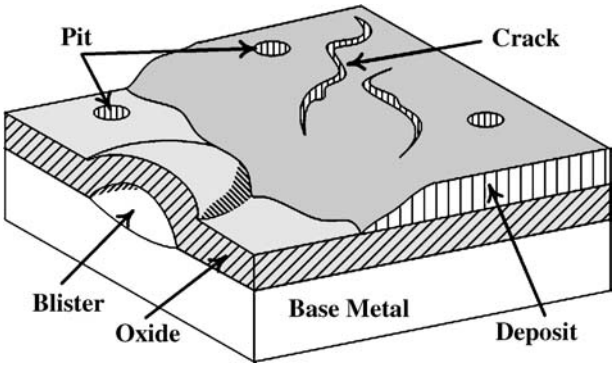

Fig. 3. A layer structure of rust

3 Framework for rusting

The transport of metallic ions and electrons plays a critical role in the formation of rust, since corrosion can be defined as an electrochemical reaction. For example, in anodic areas, iron is dissolved in seawater as ferrous ions. These ions migrate through seawater to the cathodic areas and react with some compound in seawater such as a carbonate or sulfide, to yield precipitates on metal surfaces. The opportunities to form rust increase with the number of ferrous ions absorbed. The system undergoes transition to its lowest energy state without the application of external forces if the change in free energy associated with the transition is negative. Corrosion reactions behave in exactly the same manner. The reactions are highly likely to take place to reduce the free energy of the metal (Trethewey and Chamberlain 1988). In the anodic areas, corrosion becomes stifled over a period and new anodic areas adjacent to the original ones become active. Although the propagation of corrosion is not point-to-point, it follows a kind of branching structure, as evidenced by the skeleton of corrosion pattern. Accordingly, L-systems are introduced to simulate the diffusion of rusting on metal surfaces in seawater.

Early L-systems (Hanan 1992; Lindenmayer 1968; Prusinkiewicz and Lindenmayer 1990) have been widely adopted as a general framework for plant modeling. Those systems simulated the geometry of plants under the control of endogenous or exogenous mechanisms. Although the results are impressive, the interactions between plants and their surrounding environment are neglected in most models. Prusinkiewicz et al. (1994) first introduced an environmentally sensitive L-system in 1994. The authors simulated the influence of the local environment on plant structures and behaviors, by utilizing the simple function of a turtle's position to limit the growth of plants. Based on this model, Měch and Prusinkiewicz (1996) then proposed an open L-system that incorporated a bi-directional communication module between two concurrent processes – the plant and the environment. The growth of plants is impacted by the environment, which is itself altered by the growth of the plants, through the communication module. Noser and Thalmann (1999) extended the concept to simulate living organisms in a systemic sense. They presented a behavioral animation system for humanoids. Parish and Müller (2001) also proposed a procedural approach to generate the layout of a city, depending on the user's needs. Following the new trend in open L-systems, our work presents a novel framework to simulate rusting in seawater, as guided by environmental conditions.

Figure 4 depicts the framework for rusting, in which a communication interface acts as a bridge between two major parts of the framework – the rusting module and the seawater module. The interface includes a query element and an update element, together governing the communication between these two modules. The seawater module includes a database that records present tendency distributions on the metal surface. The following section describes the tendency to rust. Environmental functions of the seawater module are stimulated by the rusting module, to evaluate or update forthcoming tendency distributions. The rusting module, itself an L-system composed of an alphabet, an initial string "axiom" and a set of production rules, simulates the evolution and the propagation of rust. At the beginning of each iterative step, the rusting module sends a message to the seawater module, stating the position of nodes (vertices of the triangular mesh), the type of rust, and the lifetime of nodes. The seawater module then determines the subsequent state of the propagation, using environmental functions limited by some criteria; the module keeps a record of the propagation. Similarly, the results of queries are returned to the rusting module. The derivation step then establishes the propagation of rust, according to the production rules of L-systems, after all feedback from the environment has been received. The rusting module then sends another message that causes the seawater module to update all tendency values of new rusty vertices and

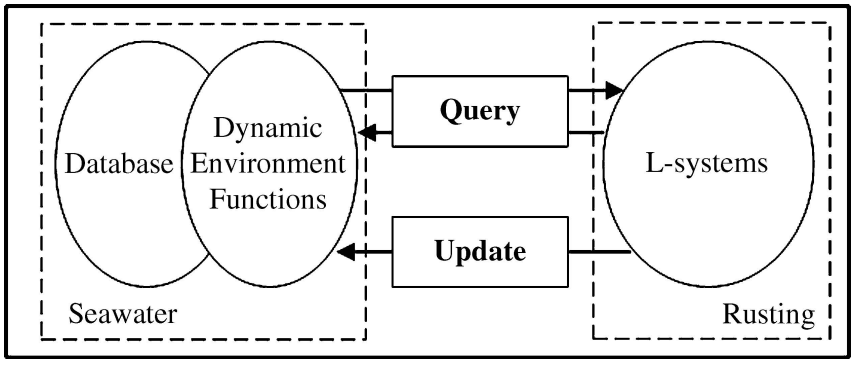

Fig. 4. A rusting framework

their neighbors before the following iteration. The proposed framework can model the complete evolution of rust in seawater by repeating this process.

4 Seawater module

Corrosion in seawater deteriorates metals by the chemical, mechanical, and biological actions of the seawater environment. A seawater module is introduced to represent the environment in which metals are immersed and corroded over a period. The primary functions of the seawater module are dynamically maintaining a record of present tendency distributions, and evaluating the propagation and evolution of rust. Whenever a query is received from the rusting module, the seawater module begins by gathering corresponding tendencies from neighboring vertices of the vertex of interest, except those at which rusting has already occurred. Rust is produced at a neighboring vertex if its tendency value exceeds both the average value of the corresponding tendency distribution and the tendency of the queried vertex. As well as determining the propagation direction of present rust, the seawater module also determines whether another type of rust is triggered. While gathering tendencies from the neighborhood, the seawater module also collects other tendencies to rust from upper layers at the queried vertex. The module triggers another type of rust that is most likely to develop at the same vertex, when the difference between the local tendency and the average of the tendency distribution exceeds the standard variation of the same distribution. The result is then attached to the message returned to the rusting module.

4.1 Tendency distribution

Recent investigations (Chandler 1985; Mercer 1990; Shreir 1976) have demonstrated that the corrosion potential of metals in seawater is a function of water salinity, temperature, oxygen content, velocity, and the surface condition of the metal. Varying one factor may change the conditions of the other factors and, in some cases, may differentially promote or suppress corrosion. Such complex properties and the composition of seawater may explain the difficulty of simulating the real mechanism of metallic corrosion in seawater. The detail of the corrosion of metals is highly complex and scientists' understanding of the process is far from complete. However, the underlying systematic distribution can be more or less observed. Thus, a tendency T, representing the potential occurrence of rust at a surface point of interest, is defined as follows (Wong et al. 1997):

$$T = \alpha * M + \beta * G + \gamma * A + \delta * O + \lambda * F + \omega * S,$$

where α, β, γ, δ, λ, and ω are weighting constants. The letters M, G, A, O, F, and S represent the maximum principle curvature, Gaussian curvature, accessibility, orientation, water current and distribution of important salts in seawater respectively. These factors can be separated into two categories: surface curvature and accessibility are local geometric properties; and orientation, currents and salt distributions are global environmental properties.

Concave areas shield a metal from current attacks, but convex areas provide more opportunities for contact with dissolved oxygen. Any sort of geometric configuration that makes the distribution of dissolved oxygen unequal may initiate corrosion. The surface curvature is frequently considered to describe surface geometric properties such as bumps, hollows and saddles. Two approaches, proposed by Turk (1992) and Calladine (1986), are adopted to estimate the principle curvature and Gaussian curvature of metal surfaces respectively, and a polygonal representation is employed to model smooth objects. Principle curvature specifies whether a point is concave or convex, and Gaussian curvature distinguishes saddle points. Surface accessibility measures how easily a surface would be touched and affects the dimensionality of the contact between an object's surface and dissolved oxygen. Miller (1994) presented a tangent-sphere method that employs a maximum sphere tangent at the vertex, without intersecting any triangles of objects, to approximate the accessibility of that vertex. Tests have demonstrated that inclined specimens corroded more than vertical specimens, and undersides corroded more than topsides (Chandler 1985). A dot product of the surface normal and the direction of gravity indicates the influence of orientation on corrosion, since an object's orientation affects the impact of currents on its surfaces. Seawater is a complex, heterogeneous environment. The distribution of significant salts in seawater that may form scales on surfaces, can not easily be measured. These scales can locally change a corrosive environment, affecting corrosion in some way. Thus, a noise solid texture is employed to describe in general the distribution of these salts in seawater. This solid texture also specifies the local variation in acidity on metallic surfaces.

The most significant feature of seawater is its movement. Turbulence, tides and seasonal currents may be present. Currents are very important in corrosion reactions, and they change surface conditions when they flow onto objects' surfaces, just as when the sun shines on objects. However, currents and sunlight differ in that, when striking an object's surface, water, unlike light, is neither absorbed nor reflected but instead exhibits a slightly altered flow direction, as it passes along the object's surface, as schematically depicted in Fig. 5a. For simplicity, an improved matte shading method with a distant area light source seems to simulate appropriately the interaction between currents and surfaces. An area light source is

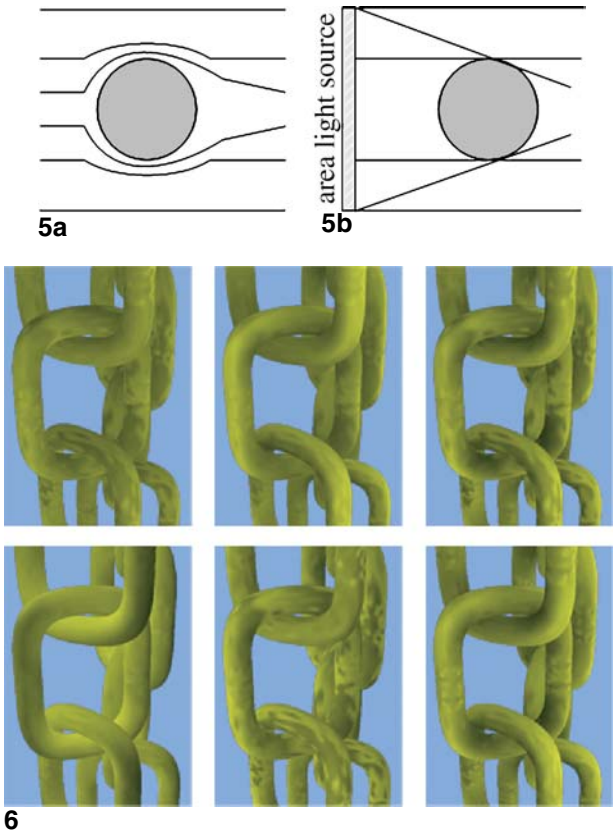

Fig. 5. The schematic diagram: **a** current; **b** area light source
Fig. 6. Tendency distributions (from *left* to *right* and *top* to *bottom*: Fe_3O_4, Fe_2O_3, blister, deposit, pit, crack)

introduced to overcome the difference between light and water in this regard. Consider Fig. 5b. The umbra on the surfaces represents a region in which the current is nearly quiet. The velocity of currents can be represented by the intensity of light in the shading model. Then the current tendency F of a vertex is defined as $F = \frac{1}{n}\sum_{i=1}^{n} I_f * (D_i \cdot N) * S(D_i, P)$, where n is the number of sample points over the light source and N is the surface normal of a vertex P. D_i is a unit vector from P to the ith sample point. The light intensity, representing current velocity, is I_f. As for normal shading, $S(D_i, P)$ represents a shadow test and a returned value of zero indicates that vertex P is in a shadow that corresponds to the ith sample point of the area light source. But, when the vertex faces directly away from the light, the returned value is set to 1. A negative value of $D_i \cdot N$ represents stationary water. Figure 6 displays experimental results of tendency distributions, where the intense yellow

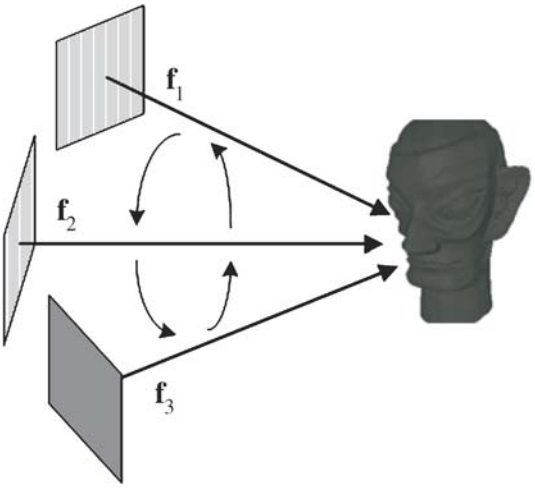

Fig. 7. A dynamic current model

represents a high tendency value and a high probability of rusting. Different tendency distributions represent preferable conditions for different types of rusting.

4.2 Dynamic tendency distribution

Several current directions are defined to describe seasonal variations, and a swing-like order simply specifies the sequence of these currents. Figure 7 depicts three current directions. The seawater module, which includes a dynamic current model, is informed to update the tendency distributions when the current changes direction. Schemes that apply the current sequence to the iteration steps cause the tendency distributions to change in the simulation, because the rusting module interprets the iterative steps as time steps (Prusinkiewicz and Lindenmayer 1990). As presented in Table 1, the water current can change direction at each consecutive or second iteration, or even less frequently. The same current can be maintained to model steady flow. Figure 8 shows the period of currents: a higher intensity of blue color represents water striking the surface more directly and a higher intensity of red color represents a quieter flow.

While the environment is essential in corrosion, the effect of the metal–environment interaction upon the environment is also important. The metallic ions formed by corrosion can affect the corrosivity of the environment. Metallic ions and electrons in a rusty area are consumed when a rusty vertex is generated, and new ions and electrons move into this area from the immediately surrounding area to achieve a new local equilibrium. The tendency values are therefore updated after each derivation step. In the seawater module, a threshold value is defined to reduce the tendency value of the new rusty vertex. The tendencies of vertices in the surrounding area also decrease according to the distance to the new rusty vertex. Figure 9 illustrates the paradigm; the red point is the new rusty vertex.

5 Rusting module

Although areas with high corrosive potential will rust severely, rusting may still occur in areas with low potential. Hence, a set of seed vertices is randomly selected from vertices at which the tendency value of the first layer exceeds a predefined threshold. A uniform random distribution is used. These vertices constitute the axiom of L-systems. When the results of queries are returned, rust development from seed vertices simultaneously proceeds along the edges connected to these vertices, according to the production rules of L-systems. The essential features of the rusting module are described by the following production rules.

Table 1. Current scheme (f_1, f_2, and f_3 represent three currents with different directions)

iteration	1	2	3	4	5	6	7	8	9	10	11	12	13	14	15
frequency = 1	f_1	f_2	f_3	f_2	f_1	f_2	f_3	f_2	f_1	f_2	f_3	f_2	f_1	f_2	f_3
frequency = 1/2	f_1	f_1	f_2	f_2	f_3	f_3	f_2	f_2	f_1	f_1	f_2	f_2	f_3	f_3	f_2
frequency = 1/3	f_1	f_1	f_1	f_2	f_2	f_2	f_3	f_3	f_3	f_2	f_2	f_2	f_1	f_1	f_1

Fig. 8. A period of currents (from left to right: f_1, f_2, f_3, f_2)

#*define* L_1 80 /* initial lifespan of apices */
#*define* P 10 /* the increment of parameter t */

initial :

$p_1 : Q(M,n,c) < A(p,l,t) : c == 1 \,\&\, t == 0 \longmapsto Q(M,0,0)A(p,l,c)$
$p_2 : Q(M,n,c) < A(p,l,t) : c == 2 \,\&\, t == 0 \longmapsto Q(M,0,0)A(p,l,c)$

termination :

$p_3 : Q(M,n,c) < A(p,l,t) : l \le 0 \;\|\; n < 0 \longmapsto R(p,l,t)$
$p_4 : Q(M,n,c) < A(p,l,t) : n == 0 \,\&\, t \ge mP \longmapsto R(p,l,t)$
$p_5 : Q(M,n,c) < A(p,l,t) : n == 0 \,\&\, t < mP \longmapsto B(p,l-1,t,T_1)$

propagation :

$p_6 : Q(M,n,c) < A(p,l,t) : c == 0 \,\&\, t\%P == 6 \longmapsto R(p,l,t)Q(M,0,c+1)$
$A(M[0],l-1,t)Q(M,0,c+1)A(M[1],l-1,t)$
$p_7 : Q(M,n,c) < A(p,l,t) : c > 0 \,\&\, t\%P == 6 \longmapsto R(p,l,t)Q(M,0,c+1)A(M[0],l-1,t)$
$p_8 : Q(M,n,c) < A(p,l,t) : c == 0 \,\&\, t\%P == 3 \longmapsto R(p,l,t)Q(M,0,0)A(M[0],l-1,t)Q(M,0,0)A(M[1],l-1,t)\cdots$
$Q(M,0,0)A(M[n-1],l-1,t)$
$p_9 : Q(M,n,c) < A(p,l,t) : c == 0 \longmapsto R(p,l,t)Q(M,0,0)A(M[0],l-1,t)Q(M,0,0)A(M[1],l-2,t)\cdots$
$Q(M,0,0)A(M[n-1],l-n,t)$

triggering :

$p_{10} : Q(M,n,c) < A(p,l,t) : c > 4 \,\&\, t\%P < 5 \longmapsto R(p,l,t)Q(M,0,0)A(M[0],l-1,t)Q(M,0,0)A(M[1],l-2,t)\cdots$
$Q(M,0,0)A(M[n-1],l-n,t)B(p,l-1,c,T_2)$
$p_{11} : Q(M,n,c) < A(p,l,t) : c == 4 \,\&\, t\%P < 4 \longmapsto R(p,l,t)Q(M,0,0)A(p,l-1,c)Q(M,0,0)A(M[0],l-1,t)Q(M,0,0)$
$A(M[1],l-2,t)\cdots Q(M,0,0)A(M[n-1],l-n,t)$
$p_{12} : Q(M,n,c) < A(p,l,t) : c == 3 \,\&\, t\%P < 3 \longmapsto R(p,l,t)B(p,l-1,c,T_2)Q(M,0,0)A(M[0],l-1,t)Q(M,0,0)$
$A(M[1],l-2,t)\cdots Q(M,0,0)A(M[n-1],l-n,t)$

$p_{13} : Q(M,n,c) : * \longmapsto \varepsilon$

torpidity&bud :

$p_{14} : B(p,l,t,d) : l \le 0 \longmapsto \varepsilon$
$p_{15} : B(p,l,t,d) : d < -1 \longmapsto B(p,l-1,t,d+1)$
$p_{16} : B(p,l,t,d) : d == -1 \longmapsto Q(M,0,0)A(p,l-1,t+P)$
$p_{17} : B(p,l,t,d) : d > 1 \longmapsto B(p,l-1,t,d-1)$
$p_{18} : B(p,l,t,d) : d == 1 \,\&\, t == 3 \longmapsto Q(M,0,0)A(p,T_3,t)$
$p_{19} : B(p,l,t,d) : d == 1 \,\&\, t == 5 \longmapsto R(p,l-1,t)$
$p_{20} : B(p,l,t,d) : d == 1 \,\&\, t == 6 \longmapsto Q(M,0,0)A(p,l-1,t)$

blistering :

$p_{21} : R(p,l,t) : t\%P == 3 \,\&\, l\%10 > 0 \longmapsto R(p,l+9,t)$

axiom : $Q(M,0,0)A(V_1,L_1,0)Q(M,0,0)A(V_2,L_1,0)\cdots Q(M,0)A(V_k,L_1,0)$

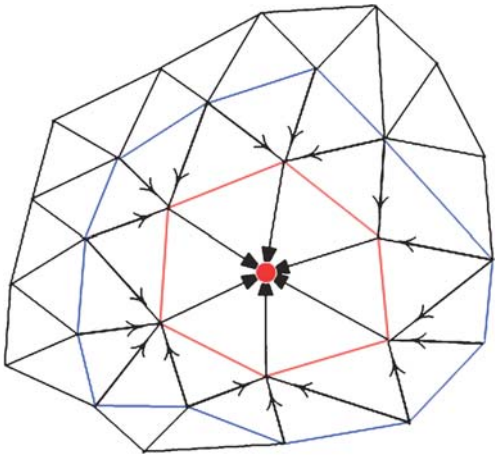

Fig. 9. Tendency reduction process

The communication symbol $Q(M, n, c)$ details a request to the seawater module and the received result of the request for deriving L-systems, where M represents an array which stores candidates for the forthcoming propagation of rust that are returned by the seawater module, and n is the number of candidates. The third parameter, c, indicates the formation of different types of rust in the upper layers. An apex A with a lifespan l denotes a cell that can continually move on the surfaces, and the parameter t denotes the type of rust. The lifespan of an apex declines gradually until it reaches zero, at which point the apex dies naturally. When rust t is formed at vertex p, a symbol $R(p, l, t)$ is introduced to outline the formation of rust.

These production rules can be divided into several parts. The initial part specifies the initialization of rust in the first layer and the termination rules govern the termination of the growth of the rust. Different types of rust develop according to different rules, as listed in the propagation set. Under the appropriate conditions, the triggering rules breed another type of rust in the upper layer. The "torpidity & bud" part describes the initial manifestation of rust or an abeyance apex. Detailed production rules follow.

Development of rust begins with a set of seed vertices $V_1, V_2, \ldots V_k$, chosen randomly, and their corresponding communication Q symbols. These seed vertices on the base metal initially transform into ferrous or ferric oxides in the first layer of rust, according to the query results returned by the seawater module. These transformations are depicted in the productions p_1 and p_2. Each derivation step begins after all query processes have been answered.

First, the rusting module checks whether the life of the apex passed, according to the context-sensitive production p_3. The module ends the growth of the apex and replaces both the apex A and the communication symbol Q by a rust node R if the lifespan equals or is less than zero. The apex is fixed at $n \leq 0$ when the seawater module determines that no space is available for new rust in the same layer. An apex should not die immediately when no proper neighbors are available to grow the same type of rust, since the seawater environment continuously varies. A period of torpidity may be entered, with a period of $|T_1|$ derivation steps due to production p_5. The constant T_1 pertains to the number of currents and the frequency of current variation. The purpose of torpidity is to halt the growth of an apex until the immediate environment changes. The symbol $B(p, l, t, d)$ locates an apex of rust t which is torpid at vertex p over $|d|$ derivation steps. Production p_4 terminates the growth in a manner similar to production p_3, when an apex has become torpid torpidity over m times.

The propagation of a crack is described by productions p_6 and p_7. A crack is generated in the stress spectrum direction with the highest intensity. Although many crack types exist, a crack may be assumed to begin and propagate in two directions. An isotropic propagation rule, p_8, explains why blisters are commonly round. The seawater module checks whether the environment at each new rusty vertex supports the breeding of another type of rust in the upper layer. Production p_9 describes the primary growth of rust that does not stimulate another type of rusting. An apex $A(p, l, t)$ with a query $Q(M, n, c)$ is replaced by a rust node $R(p, l, t)$ and many new apices A's led by query nodes Q's in each iteration. A new apex with a higher tendency has a longer lifespan than those with lower tendencies.

The rusting module follows different production rules to specify each new kind of rust triggered in upper layers. Pits and cracks are triggered by production p_{10}. Productions p_{11} and p_{12} represent the triggering of deposits and blisters respectively.

When an apex enters the torpid state, it rests for a period governed by production p_{15} and is then stimulated (by production p_{16}) to propagate again over the surfaces. In the triggering rules, the torpidity symbol B is used to sketch a bud of rust. Each bud has

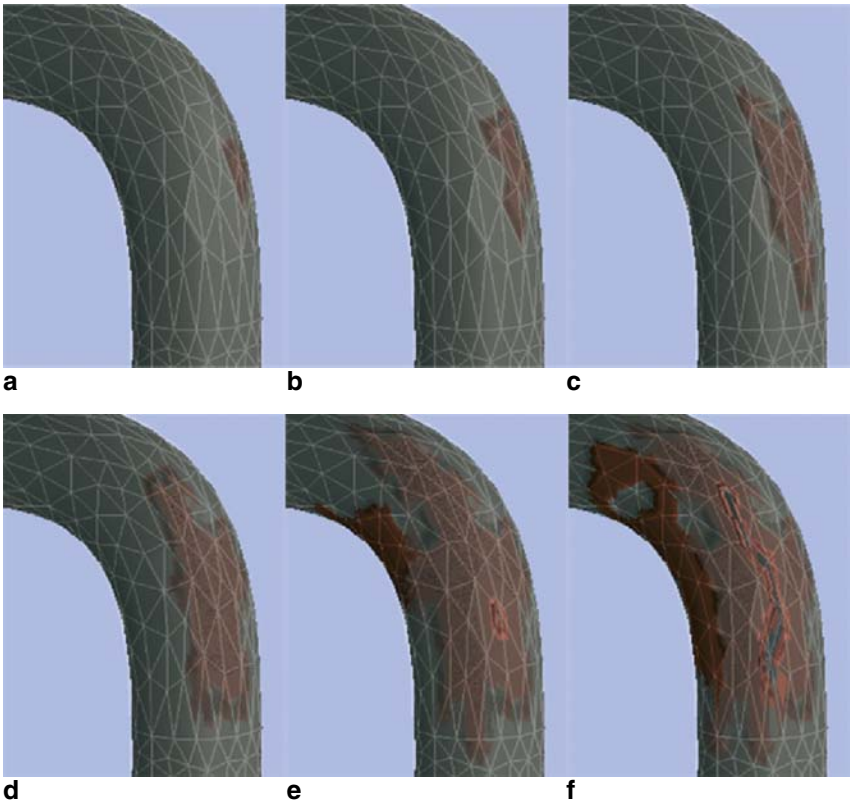

Fig. 10a–f. An example of rust development: **a** iteration 1; **b** iteration 2; **c** iteration 3; **d** iteration $3+|T_1|$; **e** iteration $3+T_2$; **f** iteration $6+T_2$

a period of T_2 derivation steps to prepare for germination (production p_{17}), because the upper rust does not necessarily appear simultaneously with the current rust. At germination, buds are replaced by nodes of different types of rust, accounted for by productions p_{18}, p_{19}, and p_{20}. Torpified apices and buds die naturally (production p_{14}).

Production p_{21} specifies the difference between blisters and other types of rust. A stimulated blister gradually swells the surface to a height that is related to the time since it began to develop. Finally, production p_{13} removes communication symbols after they have performed their tasks.

An example is used herein to describe the relationship between these sets of rules. A seed vertex is initially transformed into ferric oxide, according to production p_2, in the first layer and then diffuses outward in the same layer (production p_9), as shown in Fig. 10a,b. The bud of a crack in the upper layer is bred on the oxide, under appropriate environmental conditions (production p_{10}). The bud is present for a period (production p_{17}) and germinates according to production p_{20}, as shown in Fig. 10e. The cracking proceeds and is guided by production p_6, as depicted in Fig. 10f. An apex of ferric oxide may enter a torpid state (production p_5) during propagation, remaining dormant for a while (production p_{15}) before repropagating (production p_{16}), as illustrated in Fig. 10c,d. The growth of an apex is terminated by production p_3 when its lifespan is passed.

6 Rendering

The Whitted (1980) illumination model with a simple ray tracer, simulating the reflection and transmission of light through rust layers, is used to render the appearance of metal corroded in seawater. The

color of a point P on an object's surface is simply approximated by mixing the colors of various layers at that point. Each layer exhibits its own material structure and optical properties. A more compact layer allows less light, reflected from lower layers, to be transmitted, thereby affecting the final color of the surface. More rust may accumulate at an area with higher tendency values; the tendency distribution reasonably describes the density of rust. The coefficient of rust transmittance is adjusted according to the relative tendency values, to simulate the transmission of light through layers of varying densities. The rust constituent of a point P, at which a ray is incident, is determined on the vertices of the triangle that contains that point. Different methods of assessment are applied for different combinations of rust constituents at three triangle vertices. For example, the boundary of deposits generally crosses the middle of a triangle and pits are commonly around the vertices. Perlin's noise function and fractal subdivisions with different thresholds are adopted to determine the rust at surface points. Accordingly, the rust boundary appears to be irregular. The bottom of the pits and cracks usually contain black magnetite, while the surrounding surfaces show the characteristic red rust color of hematite. The triangle is therefore subdivided into bottom, edge and original parts to depict the features of the pits and cracks. A simple sinusoidal function is applied at the boundaries of the rust, as a bump function, to achieve the illusion of thickness, since the rust layers themselves have zero thickness. The variations of the sinusoidal function can bump up surfaces surrounding the pits and cracks where the roughness differs slightly from that of other rust. Scales, such as oxides and ferrous deposits, on surfaces generally appear rugged. The normal vectors of interior points of such rust are agitated by noise to generate uneven surfaces. Hydrogen blisters are simulated by pulling up the surface vertices some distance along their vertex normal. The blisters are located by the seawater module, and the pulling distance is proportional to the lifespan of the blister, the ratio of which is predefined. In contrast to other rusts, the blister deforms only the surface geometry and does not change the constituents of the rust.

Fig. 11. Rust on ferrous chains

7 Results

This section presents several impressive results of the approach. As shown in Fig. 11, ferrous chains are corroded in seawater under four periodically varying ocean currents with the same speed. The transition of currents is accompanied by the iteration of

Table 2. The weighting parameters of tendencies

	Max curvature	Gaussian curvature	Accessibility	Orientation	Current	Salts
Fe_3O_4	0.17	0.17	0.17	0.17	0.17	0.15
Fe_2O_3	0.2	0.1	0.3	−0.15	0.15	0.1
Blister	0.1	0.1	0.25	0.1	0.2	0.25
Deposit	−0.05	0.05	−0.2	−0.25	−0.3	0.05
Pit	0.2	0.0	0.15	−0.05	−0.3	0.3
Crack	0.15	0.3	0.2	0.0	0.25	0.1


12a


12b


13a


13b

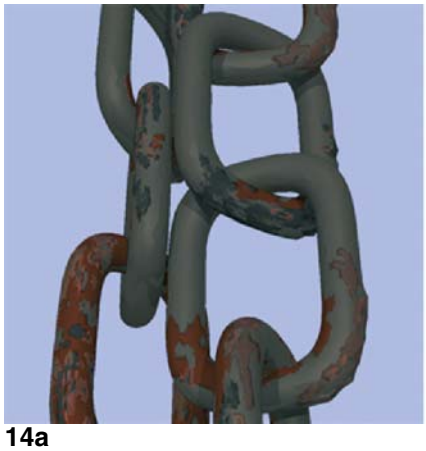
14a

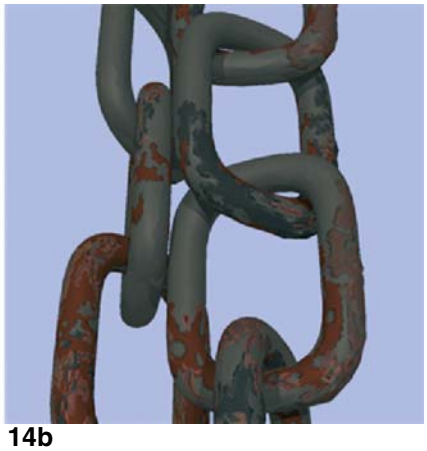
14b

Fig. 12. The difference between **a** dynamic current and **b** steady current

Fig. 13a,b. The influence of current velocity on rusting: **a** fixed velocity; **b** varied velocity

Fig. 14a,b. The results of different reduction of tendency: **a** reduction value of 0.01; **b** reduction value of 0.1

L-systems. Table 2 states the weighting coefficients of environmental and geometric factors for various types of rust. Figure 6 displays the corresponding distributions at the beginning of the simulation.

The introduction of the dynamic current model is a characteristic feature of the proposed framework. Although the variation of currents is more important than any other environmental factor, the influence

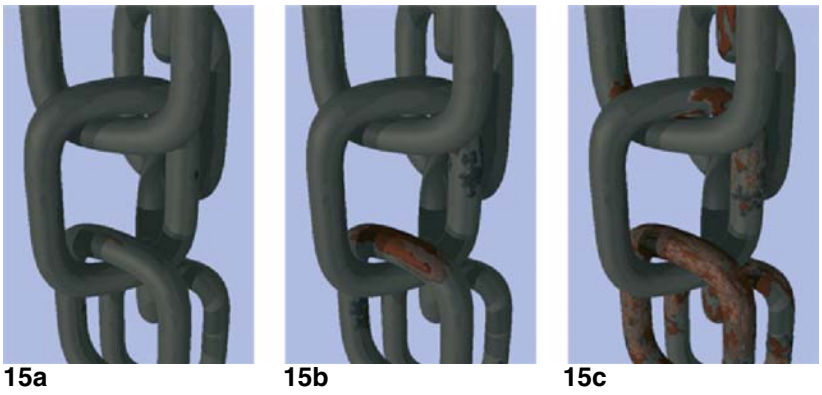
15a

15b

15c


15d


15e


15f


16a

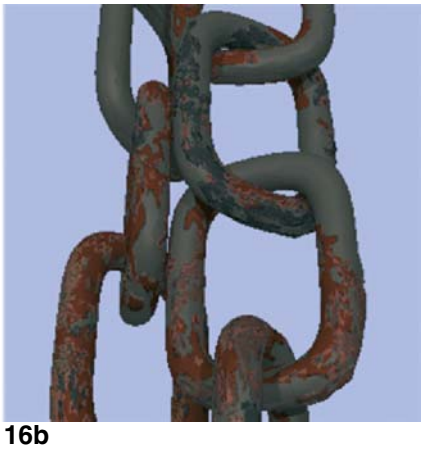
16b

Fig. 15a–f. A sequence of images corresponding to different iteration steps: **a** iteration 1; **b** iteration 5; **c** iteration 15; **d** iteration 30; **e** iteration 48; **f** iteration 69

Fig. 16a,b. Different current schemes: **a** frequency of 1/3; **b** frequency of 1

of the velocity and the direction of currents should be demonstrated. Pitting is considered to exemplify the impact of the current on the distribution of rust. Figure 12 presents the difference between the pit distributions for the dynamic current and those for the steady current. Figure 8 displays the periodic variation of ocean currents. In the case of the steady current, one of those dynamic currents is continually applied to the model, as the seawater can only flow in one direction. The surfaces sheltered from the cur-

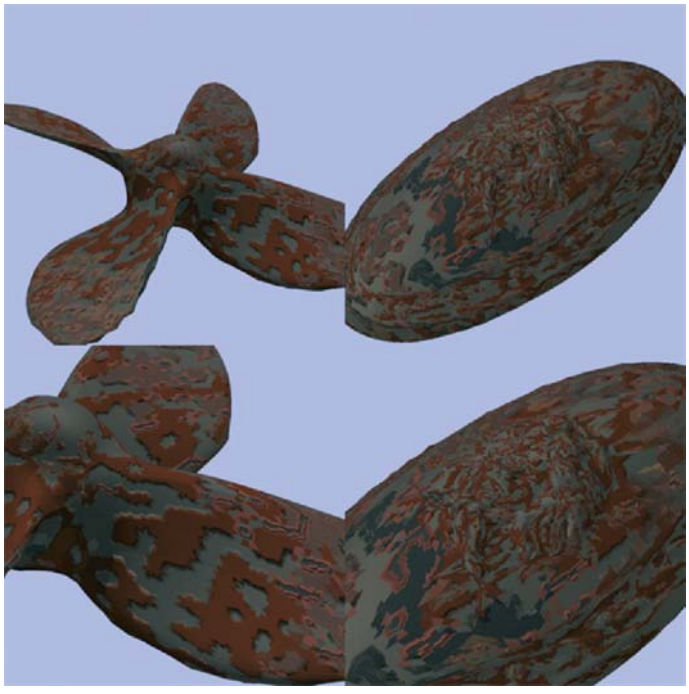

Fig. 17. Rusty objects (the *bottom row* is zooming from the *top row*)

rents may contain more pits than those facing the currents because pitting tends to be promoted by stagnant conditions. Hence, few pits are observed on the left face of the head under a steady current. More pits are observed in the example of the dynamic current, since the left face is also sheltered from the striking of current when the direction of current changes.

Figure 13 demonstrates the influence of current velocity under the same scheme of current directions. The velocity of the currents first increases as the current swings from the first direction to the last, and the velocity decreases when the current swings back. The difference is manifest only in the number of pits, and not in their distribution. Another characteristic of the proposed approach is the local variation of tendency distributions caused by the corrosion. In the seawater module, a reduction in tendency is defined to redistribute tendencies around the new rust. A reaction that involves a great reduction in free energy is more likely to happen than one that does not. Therefore, rust with a high reduction value of tendency propagates faster than that with a lower value, as illustrated in Fig. 14.

Most L-systems use the number of iterations to portray the time passed in the simulation. Figure 15 shows a sequence of images with varying numbers of iterations to illustrate aging phenomenon. Furthermore, a current may last for several iterative steps before transitioning to the next direction (Table 1). For a specific current period, corrosion at low frequency is a little slower than that at high frequency. Figure 16 indicates that different frequencies yield a slight difference in the rate and distribution of corrosion. This method also applies to other models, as shown in Fig. 17.

8 Conclusions

A physically based model for simulating the development of metallic rust development in seawater was proposed. Two modules responsible for the growth of rust and changes in the surrounding environment were elucidated, based on the framework of open L-systems. The environment determines the distributions of different instances of rust, and the corrosion changes the immediate environment. The essential feature of this model, besides its consideration of environmental influences, is that the seawater environment can change over time. The seawater module

includes a dynamic current model to characterize the periodic variation of ocean currents. Moreover, the seawater environment is characterized as a series of tendency distributions that represent the effects of seawater on rusting.

The sea is mysterious and complex, and the seawater module is not yet an exact model. Scientists do not thoroughly understand many aspects of corrosion in seawater, or in other environments. Nevertheless, many interesting research directions are available. For instance, a relevant topic is how to develop more comprehensive L-systems that can simulate different forms of corrosion, such as cavitations and crevices. Furthermore, the proposed model can be modified for a broad range of metallic corrosion processes and surrounding environments.

Acknowledgements. We would like to thank the National Science Council of the Republic of China for financially supporting this research under Contract No. NSC 90-2213-E-009-128.

References

1. Becket W, Badler NI (1990) Imperfection for realistic image synthesis. J Vis Comput Anim 1(1):26–32
2. Blinn JF (1982) Light reflection functions for simulation of clouds and dusty surfaces (SIGGRAPH '82 Proc.). Comput Graph 16(3):21–29
3. Calladine CR (1986) Gaussian curvature and shell structures. In: Gregory JA (ed) The mathematics of surfaces. Oxford University Press, Oxford, pp 179–196
4. Chandler KA (1985) Marine and offshore corrosion. Butterworths, London
5. Chang YX, Shih ZC (2000) Physically-based patination for underground objects. Comput Graph Forum 19(3):109–117
6. Craig BD (ed) (1989) Handbook of corrosion data. ASM International
7. Dorsey J, Edelman A, Jensen HW, Legakis J, Pedersen HK (1999) Modeling and rendering of weathered stone (SIGGRAPH '99 Proc.). Comput Graph 33:225–234
8. Dorsey J, Hanrahan P (1996) Modeling and rendering of metallic patinas (SIGGRAPH '96 Proc.). Comput Graph 30:387–396
9. Dorsey J, Pedersen HK, Hanrahan P (1996) Flow and changes in appearance (SIGGRAPH '96 Proc.). Comput Graph 30:411–420
10. Dorsey J, Hanrahan P (2000) Digital materials and virtual weathering. Sci Am 282(2):46–53
11. Fontana MG (1986) Corrosion engineering, 3rd edn. McGraw-Hill, New York
12. Gobron S, Chiba N (1999) 3D surface cellular automata and their applications. J Visual Comput Animat 10(3):143–158
13. Haase CS, Meyer GW (1992) Modeling pigmented materials for realistic image synthesis. ACM Trans Graph 11(4):305–335
14. Hall R (1989) Illumination and Color in Computer Generated Imagery. Springer, Berlin Heidelberg New York
15. Hanan JS (1992) Parametric L-systems and their application to the modelling and visualization of plants. PhD thesis, University of Regina
16. Heckbert PS (1986) Survey of texture mapping. IEEE Comput Graph Appl 6(11):56–67
17. Hsu SC, Wong TT (1995) Simulating dust accumulation. IEEE Comput Graph Appl 15(1):18–22
18. Jones DA (1992) Principles And Prevention of Corrosion. Macmillan, New York
19. Judd DB, Wyszecki G (1975) Color in business, science and industry, 3rd edn. Wiley, New York
20. Lindenmayer A (1968) Mathematical models for cellular interactions in development, Parts I and II. J Theoret Biol 18:280–315
21. Měch R, Prusinkiewicz P (1996) Visual models of plants interacting with their environment (SIGGRAPH '96 Proc.). Comput Graph 30:397–410
22. Mercer AD (1990) Corrosion in seawater systems. Ellis Horwood, New York
23. Merillou S, Dischler JM, Ghazanfarpour D (2001) Corrosion: simulating and rendering. In: Proceedings of Graphics Interface, pp 167–174
24. Miller G (1994) Efficient algorithms for local and global accessibility shading (SIGGRAPH '94 Proc.). Comput Graph 28:319–326
25. Newman RC, Sieradzki K (1994) Metallic corrosion. Science 263(25):1708–1709
26. Noser H, Thalmann D (1999) A rule-based interactive behavioral animation system for humanoids. IEEE Trans Visual Comput Graph 5(4):281–307
27. Parish YIH, Müller P (2001) Procedural modeling of cities (SIGGRAPH '01 Proc.). Comput Graph 35:301–308
28. Perlin K (1985) An image synthesizer (SIGGRAPH '85 Proc.). Comput Graph 19(3):287–296
29. Prusinkiewicz P, James M, Měch R (1994) Synthetic topiary (SIGGRAPH '94 Proc.). Comput Graph 28:351–358
30. Prusinkiewicz P, Lindenmayer A (1990) The algorithmic beauty of plants. Springer, Berlin Heidelberg New York
31. Rogers TH (1971) Marine corrosion.
32. Ross TK (1977) Metal corrosion. Oxford University Press, Oxford
33. Shreir LL (ed) (1976) Corrosion: metal/environment reactions. Newnes-Butterworths, London
34. Touloukian YS (1967) Thermophysical properties of high temperature solid materials. Macmillan, New York
35. Trethewey KR, Chamberlain J (1988) Corrosion for students of science and engineering. Wiley, New York
36. Turk G (1992) Re-tiling polygonal surfaces (SIGGRAPH '92 Proc.). Comput Graph 26(2):55–64
37. Warniers R (1998) Dirty pictures. Comput Graph World 21(6):51–60
38. Whitted T (1980) An improved illumination model for shaded display. Commun ACM 23(6):343–349
39. Wong TT, Ng WY, Heng PA (1997) A geometry dependent texture generation framework for simulating surface imperfections. In: Proceedings of Eurographics Workshop on Rendering, pp 139–150

YAO-XUN CHANG obtained his BS degree in applied mathematics from National Chung Hsing University, Taiwan, in 1993. He is currently a PhD candidate in the Department of Computer and Information Science at National Chiao Tung University, Taiwan. His research interests are in the area of procedural texture synthesis, virtual reality and non-photorealistic rendering.

ZEN-CHUNG SHIH was born on 10th February 1959, in Taipei, Taiwan, Republic of China. He received his BS degree in Computer Science from Chung-Yuan Christian University in 1980, MS degree in 1982 and PhD degree in 1985 in computer science from the National Tsing Hua University. Currently, he is a professor in the Department of Computer and Information Science at the National Chiao Tung University in Hsinchu. His current research interests include procedural texture synthesis, non-photorealistic rendering, global illumination, and virtual reality.